*** This journal is indexed in the Scientific Information Database (http://en.journals.sid.ir/JournalList.aspx?ID=3998).**
*** This journal is indexed in the Iranian Magazines Database (www.magiran.com/maginfo.asp?mgID=4585).**
*** This journal is indexed in the Islamic World Science Citation Center (http://ecc.isc.gov.ir/showJournal/3561).**

Language Editor: Sajjad Saberi

Art & Design: Fatemeh Hajizadeh

Iranian Association of Chemical Engineers, Unit 11, No. 13 (Block 3), Maad Building, Shahid Akbari Boulevard, Azadi Ave., Tehran - Iran.

Tel: +98 21 6604 2719 **Fax:** +98 21 6602 2196

Iranian Journal of Chemical Engineering

Vol. 15, No. 1 (Winter 2018), IAChE

Iranian Journal of Chemical Engineering
Vol. 15, No. 1 (Winter 2018), IAChE

A Comprehensive Numerical Simulation of a Low-Temperature Fischer-Tropsch Synthesis in a Fixed Bed Reactor in Trickle Flow Regime

H. Salimi, Sh. Shahhosseini [*]

School of Chemical, Petroleum and Gas Engineering, Iran University of Science and Technology, P. O. Box: 16765-163, Tehran, Iran

ARTICLE INFO

Article history:
Received: 2016-06-27
Accepted: 2017-01-10

Keywords:
LTFT Synthesis
Fixed Bed Reactor
Mass Transfer Restrictions
2D-Multiphase
Heterogeneous Model
Numerical Simulation

ABSTRACT

Gas to liquid (GTL) process involves heterogeneous catalytic chemical reactions that convert synthesis gas to hydrocarbons and water vapor. Fischer-Tropsch synthesis, as the heart of the process, is a three-phase chemical phenomenon that includes gaseous phase-synthesis gas, light hydrocarbons and water vapor, liquid phase–heavy hydrocarbons, solid phase-catalyst and wax products. The presence of liquid phase in catalytic packed bed in LTFT synthesis causes mass transfer restrictions and affects the reaction conversion. In this work, a numerical simulation of the LTFT fixed bed reactor in trickle flow regime has been accomplished using numerical computation codes to understand the impact of liquid phase on the reactor performance. For this purpose, we have developed an axisymmetric two-dimensional multiphase heterogeneous model where syngas, containing carbon monoxide and hydrogen, can be transferred into the liquid phase. The reactor consists of a shell and tube that filled with a spherical cobalt catalyst. Reaction conditions are as follows: a wall temperature of 473 K, a pressure of 20 bars, and a gas hour space velocity (GHSV) of 111 $Nml.g_{cat}^{-1}.h^{-1}$. Numerical simulation results proved the negative impact of liquid presence on the reaction conversion. Model predictions were examined against reported experimental and numerical pseudo-homogeneous model, and it was found that applying the heterogeneous, instead of pseudo-homogeneous, model decreases clearly the deviation of numerical results from experimental data. Thus, assuming the single-phase flow in LTFT synthesis is not always true.

1. Introduction

In recent years, the availability of natural gas resources and improvements to the exploration of more resources provided a momentum to use the gas to liquid (GTL) technology. In this process, natural gas is first converted to the synthesis gas, which mainly consists of carbon monoxide and hydrogen, and then a mixture of linear hydrocarbons is produced via the catalytic Fischer-Tropsch

[*]Corresponding author: shahrokh@iust.ac.ir

synthesis (FTS) reactions.

FTS reactions are polymerization reactions and produce olefinic and paraffinic hydrocarbons as follows:

$$CO + \left(\frac{2n+1}{n}\right) H_2 \rightarrow \left(\frac{1}{n}\right) C_nH_{2n+2} + H_2O \qquad (1)$$

$$CO + 2H_2 \rightarrow \left(\frac{1}{n}\right) C_nH_{2n} + H_2O \qquad (2)$$

FTS reactions with $\Delta H = -168\ kj/mol$ are highly exothermic, and their chemistry is complex due to the polymeric nature and produces a wide range of gaseous, liquid, and solid hydrocarbons. FTS produces some fuels of high quality due to the absence of sulfur compounds and aromatics. Depending on the desirable products, FTS process can be run either at low temperature (200-250 ℃) (LTFT), where pressure is above 20 bar, or at high temperature (HTFT), operating at 300-350 ℃ and 15-20 bar. For the FTS process, several metal-based catalysts can be used; however, in an industrial application, only iron and cobalt catalysts appear to be economically feasible. Iron-based catalysts are generally used with the CO-rich syngas produced from coal gasification with water-gas shift activity, whereas cobalt-based catalysts are more commonly used with H_2-rich syngas produced by natural gas steam reforming [1]. Iron-based catalysts are used in HTFT process that mainly produces gasoline, and cobalt-based catalysts are used in LTFT process that mainly produce heavier hydrocarbons such as diesel and wax products [2, 3]. Due to a better intrinsic activity, higher selectivity to linear long-chain paraffins, negligible water-gas shift activity, and low oxygenates selectivity, cobalt-based catalysts have been successfully applied to the industrial processes. Three types of the reactors, including multi-tubular fixed bed reactor, slurry bubble column reactor, and fluidized bed reactors have been employed for FTS process [4]. Each reactor type has its own advantages and disadvantages. For example, in slurry bubble column and fluidized bed reactors, the catalysts collide with each other causing erosion to each other. These reactor types are superior in heat transfer compared with fixed-bed reactors and induce lower pressure drop. Fixed-bed reactors are simple to build and operate, and the catalyst pellets experience no attrition during the operation [1,3]. On the other hand, pressure drop in fixed-bed reactors is relatively high. The fixed-bed FTS process, as one of the most competing reactor technologies, occupies a special position in FTS industrial processes [4].

2. Background

The LTFT synthesis involves a three-phase phenomenon. The gas phase contains the syngas and water vapor and gaseous light hydrocarbon products. The liquid phase includes higher hydrocarbons, where the solid phase consists of the catalyst pellets and wax products [5].

In contrast to slurry-phase FTS reactors, the literature on the packed bed FTS reactor modelling and simulation is very limited. In 1980, Bub et al. [6] used a two-dimensional pseudo-homogeneous model to predict a product distribution and a conceptual design of a fixed bed reactor that converts nitrogen-rich syngas. Atwood and Bennet [7] proposed a heterogeneous one-dimensional plug flow model to investigate the effects of operational parameters on the industrial reactors. Liu et al. [8] applied a two-dimensional dynamic heterogeneous model to a catalytic fixed bed FTS reactor. Wang et al. propsoed a one-dimensional heterogeneous model to simulate fixed bed FTS reactor for hydrocarbon

production [9]. Jess and Kern [10] developed a two-dimensional pseudo-homogeneous model for primary studies on the use of nitrogen-rich syngas. De Swart et al. [11] developed a one-dimensional, heterogeneous model for packed bed reactors with a cobalt catalyst. Moutsoglou and Sunkara [12] proposed a more comprehensive numerical simulation model to evaluate FTS in a tubular multi-tube reactor packed with the iron-based catalyst. The effects of the process parameters on product distribution were also investigated. Jess and Kern [13] further developed a two-dimensional, pseudo-homogeneous model of a fixed packed bed reactor with a pore diffusion limitation for both iron and cobalt catalysts, utilizing boiling water as the coolant [14]. Jens et al. [15] proposed a one-dimensional pseudo-homogeneous model for LTFT synthesis on a cobalt based catalyst. In this model, only gas phase has been assumed to be the flowing phase, and the influence of the liquid film around the catalyst pellets has been modeled by considering the rate of the reactant mass transfer from the gas phase into static liquid film. They used this model to investigate the heat transfer rate of a channel-type reactor and the effect of the catalyst on the reactor performance. In addition, in 2009, Robert et al. [3] developed a one-dimensional pseudo-homogeneous model for numerical simulation of LTFT synthesis. Considering axial diffusion of the species as the major difference of their model with other models, they also assumed that the reactor worked in a trickle flow regime and solved the conservation equations for both liquid and gas as the flowing phases.

Although, in most FTS mathematical modelling and numerical simulations, only gas is assumed to be the flowing phase; in real conventional LTFT operating condition, there is a trickle flow regime in the reactor, such that the gaseous and liquid phases flow down through the catalytic bed. In fact, the heavy hydrocarbons are in the liquid phase, and water vapor along with light hydrocarbons and unreacted syngas are in the discharging gas phase [4, 14, 15]. In this condition, the liquid products fill the pores of the catalysts and form a film around it. Therefore, both internal and external mass transfer diffusion rates restrict the motion of the syngas to the catalyst active sites and decrease the reaction conversion rate. To prevent intra particle mass transfer limitations, fine and equal catalyst pellets, in the micron scale, should be used. This catalyst size is inappropriate for use in the industrial packed bed reactors due to unacceptable pressure drop [16]. A way to prevent the extreme internal mass transfer limitations is to use eggshell catalysts [17-20]. In the industrial applications, it is reported that eggshell catalysts are a very attractive solution to eliminating intra particle limitations in FTS fixed bed reactors [20]. It weakens the influence of the internal diffusion and leads to an increase in the desired product selectivity, although simultaneously reduces the active catalyst content and total reactor yield [21].

Most of the researchers assume that the mass transfer resistance caused by the liquid film on the outer surface of the catalyst is negligible compared to the mass transfer resistance caused by the liquid-filled pores [1, 16, 17, 20, 22, 23]. However, in some cases, ignoring the external mass transfer limitations leads to the unacceptable errors between the numerical modeling results and the experimental data. Vadim et al. [24] announced that, in low GHSV, the role of external liquid film on the catalyst surface is

significant and ignoring it causes an error of around 20 %. In addition, Robert et al. [3], in 2009, taking into account both pore and film diffusion limitations, reported that the influence of these two factors is comparable.

Along with the development of the numerical techniques to solve complicated problems, the use of computational fluid dynamics (CFD) has been attended in Fischer-Tropsch reactor simulation. The aim of this work is to numerically simulate a LTFT packed bed reactor in a trickle flow regime to further understand the impact of the liquid phase on the reactor's performance. For this purpose, the mass transfer from the gas phase to the liquid phase has been considered.

3. Mathematical modelling

To simulate a tubular fixed bed Fischer-Tropsch reactor, an axisymmetric two-dimensional multi-phase heterogeneous model has been developed. The schematic diagram of the system is given in Figure 1.

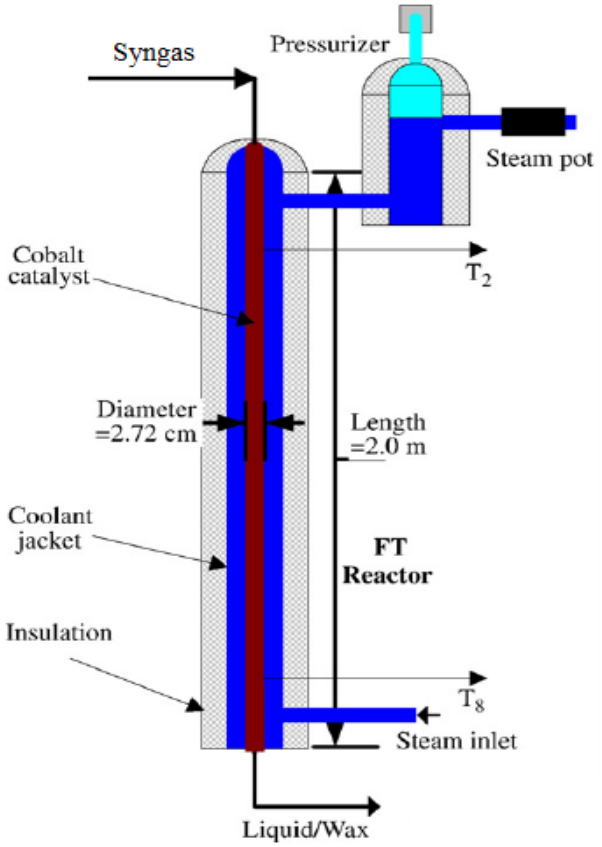

Figure 1. Schematic diagram of a tubular reactor [23].

The reactor is a vertical tube with 2 m in length, 27.2 mm in diameter, and 3 mm in wall thickness. As shown in this figure, the syngas, containing hydrogen and carbon monoxide, enters the reactor at the top and flows downwards. The reaction products along with the unreacted syngas exit the reactor outlet at the bottom. The reactor is packed with the spherical catalyst pellets, and pressurized water is circulated around it to remove the heat of the reactions. The flow inside the reactor is modelled as a two-phase flow through the packed bed of the solid catalyst particles that represents a porous medium. Physical properties and operating conditions are listed in Table 1.

Table 1
Physical properties and operating conditions.

Reactor type	Shell and tubes, focused on a single tube
Catalyst type	Co-based
Catalyst shape	Spherical
Catalyst size	3 mm
Bulk density	700 $kg.m^{-3}$
I.D. of the single tube	27.2 mm
Length of tube	2 m
Operating pressure	20 bar
GHSV (feed)	111 ($Nml.g_{cat}^{-1}.h^{-1}$)
Inlet & coolant temp.	473 k
Inlet H_2/CO molar ratio	2

The main assumptions employed in the current model for the FTS numerical modelling are listed as follows:

- Reynolds number was calculated using the mean diameter of the spherical pellets and, accordingly, a laminar flow was assumed.
- The tube geometry was assumed to be two-dimensional and axisymmetric.
- All of the operational parameters such as productivity, selectivity, conversion, etc. did not change over time due to a steady-state assumption.
- The gas phase was composed of the syngas, the light hydrocarbon products, and water vapor.
- The liquid phase, formed during the process, was composed of heavy hydrocarbon products.
- The light hydrocarbons consisted of C1-C4
- The heavy hydrocarbons (heavier than butane) have been considered as C5+.
- The solid hydrocarbon products in the form of wax were neglected.
- Only CO and H_2 were transferred from the gas mixture to the liquid phase.
- The catalytic bed was assumed to be statistically uniform and no channeling with isotropic hydrodynamic properties occurred.
- Because of small amounts of oxygenates (alcohols, etc.), compared to those of hydrocarbons, the production of these compounds was neglected.

3.1. The hydrodynamic model

3.1.1. The continuity equations

It is pointed out that the flow type in the FTS packed reactor is in the form of liquid products trickling through the catalytic bed [25]. In this work, the Eulerian-Eulerian approaches, which consider each phase as an interpenetrating continuum, has been applied to the trickling liquid flows. The continuity equations for the gaseous and liquid phases are respectively shown below:

$$\frac{\partial}{\partial t}(X_G \rho_G) + \nabla.(X_G \rho_G \vec{v}_G) = -\dot{m}_{GL} \quad (3)$$

$$\frac{\partial}{\partial t}(X_L \rho_L) + \nabla.(X_L \rho_L \vec{v}_L) = +\dot{m}_{GL} \quad (4)$$

And:

$$X_G + X_L = 1 \quad (5)$$

In the above equations, G and L subscripts represent gas and liquid phases, respectively. X, ρ, $\vec{v}$ represent volume fraction, density, and velocity vector relevant to the corresponding phase, respectivily. $\dot{m}_{GL}$ is the mass transfer rate from gas phase to liquid phase, modelled by Henry's law [26].

3.1.2. The momentum equations

Similar to the continuity equation, momentum equations were considered separately for each phase:

$$\frac{\partial(\mathrm{X_G}\rho_\mathrm{G}\vec{\mathrm{v}}_\mathrm{G})}{\partial \mathrm{t}} + \nabla.(\mathrm{X_G}\rho_\mathrm{G}\vec{\mathrm{v}}_\mathrm{G}\vec{\mathrm{v}}_\mathrm{G}) = -\mathrm{X_G}\nabla \mathrm{p} + \nabla.(\bar{\bar{\tau}}_\mathrm{G}) + \mathrm{X_G}\rho_\mathrm{G}\vec{\mathrm{g}} + \vec{\mathrm{R}}_\mathrm{LG} - \dot{\mathrm{m}}_\mathrm{GL}\vec{\mathrm{v}}_\mathrm{G} + \vec{\mathrm{F}}_\mathrm{G} \quad (6)$$

$$\frac{\partial(\mathrm{X_L}\rho_\mathrm{L}\vec{\mathrm{v}}_\mathrm{L})}{\partial \mathrm{t}} + \nabla.(\mathrm{X_L}\rho_\mathrm{L}\vec{\mathrm{v}}_\mathrm{L}\vec{\mathrm{v}}_\mathrm{L}) = -\mathrm{X_L}\nabla \mathrm{p} + \nabla.(\bar{\bar{\tau}}_\mathrm{L}) + \mathrm{X_L}\rho_\mathrm{L}\vec{\mathrm{g}} + \vec{\mathrm{R}}_\mathrm{GL} + \dot{\mathrm{m}}_\mathrm{GL}\vec{\mathrm{v}}_\mathrm{G} + \vec{\mathrm{F}}_\mathrm{L} \quad (7)$$

In equations 6 and 7, $\vec{F}_G$, $\vec{F}_L$, and $\bar{\bar{\tau}}_G$, $\bar{\bar{\tau}}_L$ represent the sink terms caused by tehpacked bed and stress tensors, respectively. Furthermore, $\vec{R}_{LG}$ and $\vec{R}_{GL}$ are the exchanged momentum between the phases due to contact among them.

In this work, a porous medium model is developed that considers the solid phase as a momentum sink for the catalytic packed bed. For the homogeneous porous medium model, a general momentum sink term is given by:

$$\mathrm{F} = -\left(\frac{\mu}{\alpha}\mathrm{v_i} + \mathrm{C_2}\frac{1}{2}\rho|\mathrm{v}|\mathrm{v_i}\right) \quad (8)$$

where μ is molecular viscosity, α and C_2 are permeability coefficient and inertial resistance coefficient, respectively, which are explained as follows:

The momentum sink term is composed of two parts: A viscous loss term (dominant in a laminar flow, based on Darcy's law) and an inertial loss term (dominant in a high velocity flow). The permeability factor (inverse of viscous loss term) and inertial resistance can be calculated from the semiempirical Ergun equation:

$$\alpha = \frac{\mathrm{d_p^2}\varepsilon^3}{150(1-\varepsilon)^2} \quad (9)$$

$$\mathrm{C_2} = \frac{3.5(1-\varepsilon)}{\mathrm{d_p}\varepsilon^3} \quad (10)$$

where ε and d_p are the bed porosity and mean particle diametere, respectively.

3.1.3. The energy equations

The energy equations for each gas and liquid phases are as follows:

$$\frac{\partial}{\partial t}[\varepsilon X_G\rho_G E_G + (1-\varepsilon)\rho_s E_s] + \nabla.[\vec{v}_G X_G(\rho_G E_G)] = \nabla.\left[k_{eff}^G\nabla T - (\textstyle\sum_i h_i^G J_i^G)\right] + S_G + Q_{LG} - \dot{m}_{GL}h_G \quad (11)$$

$$\frac{\partial}{\partial t}[\varepsilon X_L\rho_L E_L + (1-\varepsilon)\rho_s E_s] + \nabla.[\vec{v}_L X_L(\rho_L E_L)] = \nabla.\left[k_{eff}^L\nabla T - (\textstyle\sum_i h_i^L J_i^L)\right] + Q_{GL} + \dot{m}_{GL}h_G \quad (12)$$

In the above equations, subscripts s' and 'i' are relative to the solid porous media and the ith component in the mixtures. In addition, E, h, J, and S are the total energy, enthalpy, mass diffusion flux, and the source term flux due to the reaction heat, respectively. Moreover, Q_{LG} and Q_{GL} represent the heat transfer flux between the phases and

$$Q_{LG} = -Q_{GL} \quad (13)$$

Furthermore, k_{eff} is the effective thermal conductivity calculated by the below equation.

$$k_{eff} = \varepsilon k_G + (1-\varepsilon)k_s \quad (14)$$

3.1.4. The species transport equation

The species transport equation for the gas or liquid phase is given by:

$$\frac{\partial(X_G\rho_G Y_i^G)}{\partial t} + \nabla.\left(X_G\rho_G\vec{v}_G Y_i^G\right) = -\nabla.X_G\vec{J}_i^G + X_G R_i^G - \dot{m}_{GL}^i + \mathcal{R} \quad (15)$$

$$\frac{\partial(X_L\rho_L Y_i^L)}{\partial t} + \nabla.(X_L\rho_L\vec{v}_L Y_i^L) = -\nabla.X_G\vec{J}_i^L - \dot{m}_{GL}^i + \mathcal{R} \quad (16)$$

where Y_i is the mass fraction of the i^{th} component in its phase, and $\mathcal{R}$ represents the heterogeneous raction rate.

3.1.5. The pressure drop calculation

The Ergun equation for isotropic packed beds was applied to calculate the pressure drop.

$$\frac{dp}{dx} = \frac{150\mu}{{d_p}^2}\frac{(1-\varepsilon)^2}{\varepsilon^3}v_\infty + \frac{1.75\rho}{d_p}\frac{1-\varepsilon}{\varepsilon^3}v_\infty^2 \quad (17)$$

3.2. The reaction model

3.2.1. The reaction rate

As mentioned earlier, Fischer-Tropsch synthesis produces a wide range of the hydrocarbons such as saturated and unsaturated compounds and, in some cases, the oxygenate due to the side reactions. Therefore, it is difficult to consider all of the reactions due to the sharp increase in computational time and cost. Therefore, for simplification, the production reactions of $C_1 - C_4$ are considered directly, and the next products have been estimated by a pseudo material equation called C_{5+} [27].

$$2CO + 5H_2 \rightarrow C_2H_6 + 2H_2O \quad (18)$$

$$3CO + 7H_2 \rightarrow C_3H_8 + 3H_2O \quad (19)$$

$$4CO + 9H_2 \rightarrow C_4H_{10} + 4H_2O \quad (20)$$

$$6.05CO + 13.1H_2 \rightarrow C_{6.05}H_{14.1}(C_{5+}) + 6.05H_2O \quad (21)$$

The overall reaction rate of FTS is given by [28]:

$$r_{FT} = \frac{a.\exp\left(\frac{-E_a}{RT}\right).C_{CO}.C_{H_2}}{\left[1+b.\exp\left(\frac{-E_a}{RT}\right).C_{CO}\right]^2} \quad (22)$$

In particular, for each product:

$$r_{C_1} = d.\exp\left(\frac{-E_d}{RT}\right).r_{FT} \quad (23)$$

$$r_{C_2} = e.\exp\left(\frac{-E_e}{RT}\right).r_{FT} \quad (24)$$

$$r_{C_3} = \beta.r_{C_2} \quad (25)$$

$$r_{C_4} = \beta.r_{C_3} \quad (26)$$

$$r_{C_{5+}} = \beta.r_{FT} \quad (27)$$

where β is the chain growth probability constant and, according to Anderson-Schulz-Flory (ASF), distribution model was fixed to 0.784 [23].

The other kinetic parameters are listed in Table 2.

Table 2
Kinetics parameters.

$a\ (m^6.mol^{-1}.g_{cat}^{-1}.s^{-1})$	$E_a\ (kJ.mol^{-1})$	$b\ (m^3.mol^{-1})$
26.77	100	3.69
$E_b\ (kJ.mol^{-1})$	$c\ (m^3.g_{cat}^{-1}.s^{-1})$	$E_c\ (kJ.mol^{-1})$
20	680483	145
d	$E_d\ (kJ.mol^{-1})$	e
2.08×10^8	81	6.65×10^3

3.2.2. The conversion and selectivity

The conversion of the reactants was calculated as follows:

$$x_i = \frac{F_{i,in} - F_{i,out}}{F_{i,in}} \quad (28)$$

The selectivity of all of the hydrocarbon products was calculated as:

$$s_i = \frac{\text{no. of moles of product formed} \times \text{no. of C atoms present}}{\text{no. of moles CO consumed}} \quad (29)$$

Furthermore, the product efficiency was calculated as:

$$\mathrm{Pr_i} = \frac{\text{g.of product formed}}{\text{g.of catalyst used}\times\text{time}} \qquad (30)$$

4. Numerical solution method

As mentioned in section 1, sophisticated heterogeneous catalytic reaction equations that are intensively coupled with those of two-phase flow in a catalytic packed bed, together with the concurrent heat and mass transfer equations make the Fischer-Tropsch process model very complex. Therefore, it is a challenging task to apply a numerical computation to solve the equations. A comprehensive numerical simulation of this process, containing the entire aspects of the system, can provide some guidance for the scale up, design, and optimization of a fixed bed F-T reactor.

The Finite Volume Method was used to discretize the governing equations with corresponding initial and boundary conditions described in section 3. A pressure-based solver utilizing the SIMPLE algorithm was applied to the pressure velocity coupling scheme. Laminar flow regime was assumed due to the very tiny scale pathways created through the small spherical catalyst pellets. The Eulerian approach was used for the two-phase flow through the porous media. To achieve higher accuracy, the second-order upwind scheme was used to discretize the partial differential equations, except for the volume fraction equation where the QUICK scheme was applied.

5. Results and discussion

5.1. Results

Variation of the desired product reaction rate is shown in figure 2. This figure indicates, at the reactor entrance, owing to the high syngas concentration, that the reaction rate is also high, although it is reduced along the reactor length due to the decline of syngas concentration.

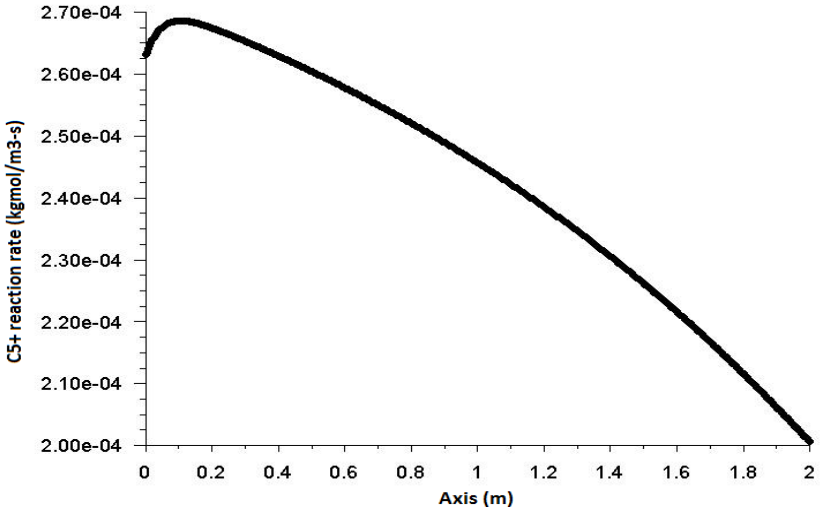

Figure 2. Heterogeneous reaction rate of C5+ against reactor axis.

Figure 3 represents the simulated temperature profile along the reactor axis. The high reaction rate at the reactor inlet also means that the heat production is high.

In a similar manner to reaction rate, due to the high concentration of the reactants in the feed stream, initially, temperature rises to a maximum value and, then, is reduced with consumption of the reactants and decreases in heat production rate.

Volume fraction of the liquid phase (C_{5+}) is shown in Figure 4. The liquid phase is

accumulated during the process as a heterogeneous reaction product, and there is no liquid phase in the feed. Due to gravity, the liquid moves towards the bottom of the reactor, and its volume fraction increases along the reactor length.

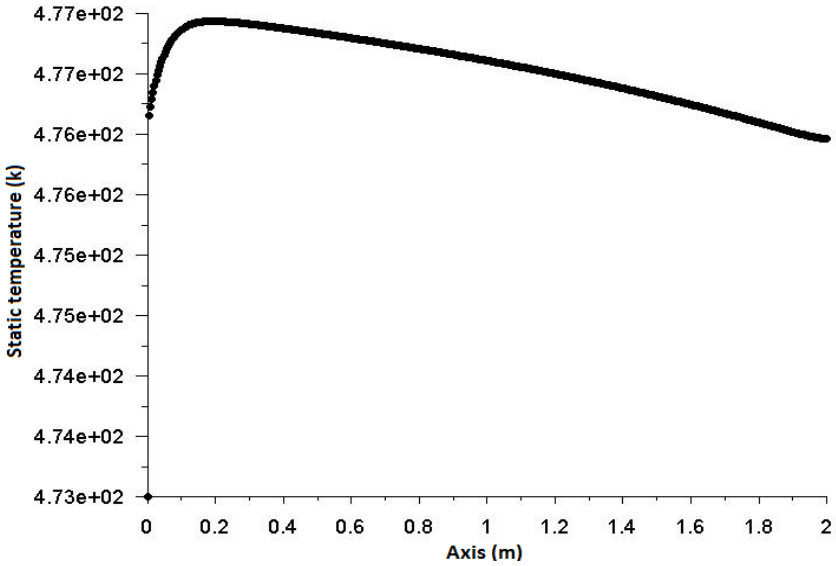

Figure 3. Static temperature against reactor axis.

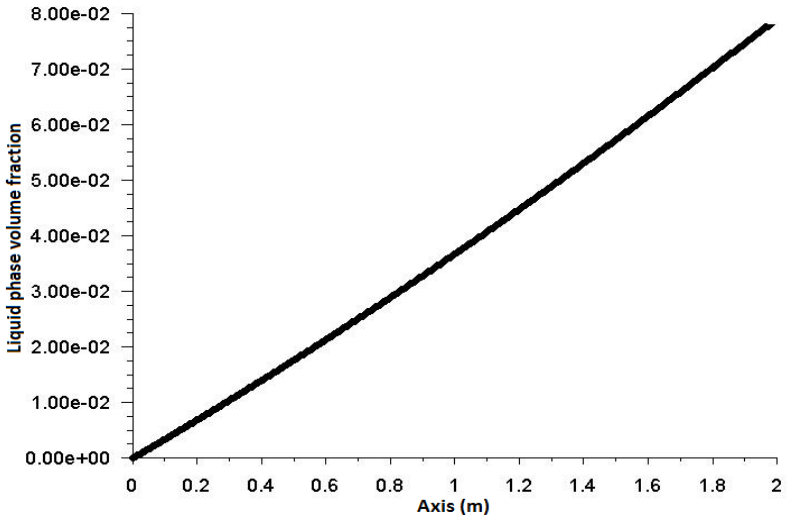

Figure 4. Volume fraction of the liquid phase against the reactor axis.

As previously explained, dissolution of the synthesis gas into the liquid phase was used to model the effect of the liquid film around the catalyst pellet on the reaction conversion. The model predictions indicate that the liquid phase mass transfer resistance lowers the reaction conversion rate preventing a part of the reactants (carbon monoxide and hydrogen) to reach the catalyst surface and get out from the bottom of the reactor along with the desired product. Figure 5 represents the mass transfer rates of carbon monoxide and hydrogen along the reactor axis.

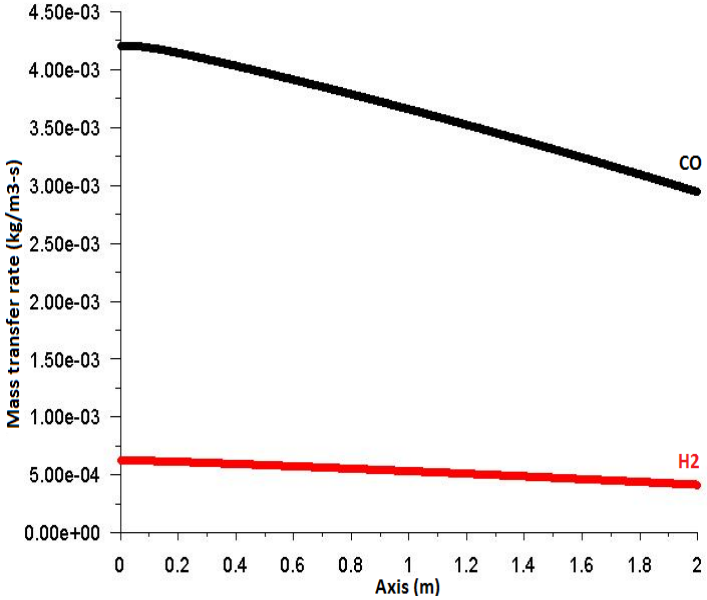

Figure 5. Mass transfer rate of reactants.

Due to the absence of the syngas in the liquid phase and its high concentration in the feed, the mass transfer driving force is maximum at the reactor entrance. With consumption of the syngas by the reactions, concentrations of hydrogen and carbon monoxide decrease in the gas phase along the reactor axis. At the same time, the liquid phase accumulation along the reactor axis leads to a decrease in the mass transfer rates.

Pressure drop profile on the reactor axis is shown in Figure 6. According to the Ergun equation, there is a direct relationship between the pressure drop on the one hand and reactor length and feed velocity on the other hand. Since the reactor length is short and its GHSV is low in comparison with the industrial packed bed reactors, the pressure drop is also low.

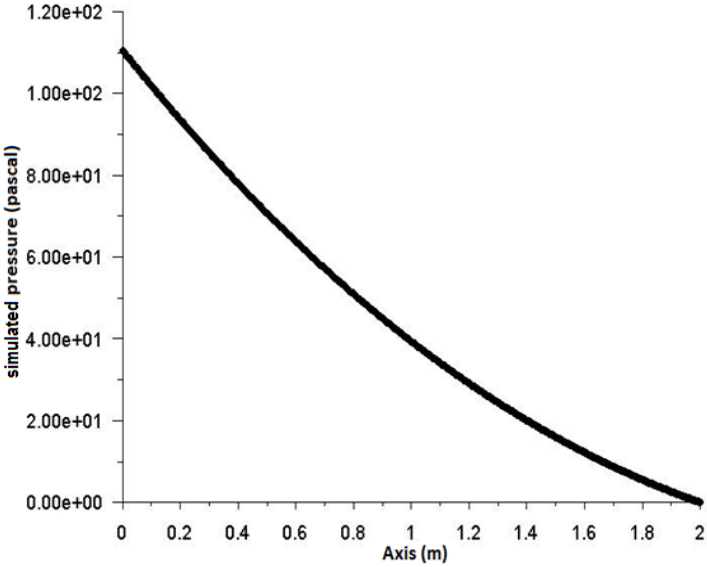

Figure 6. Static pressure along the reactor axis.

Figure 7 shows the variation of CO and H_2 conversion rates along the reactor axis. According to this figure, syngas conversion rate is zero at the reactor inlet and increases in a linear trend towards the reactor outlet. This figure also shows a comparison made between the simulated values of conversion rates at outlet of the reactor and the corresponding experimental data of Rafiq et al. [23]. The comparison indicates that the model has been able to predict the data with reasonable accuracy.

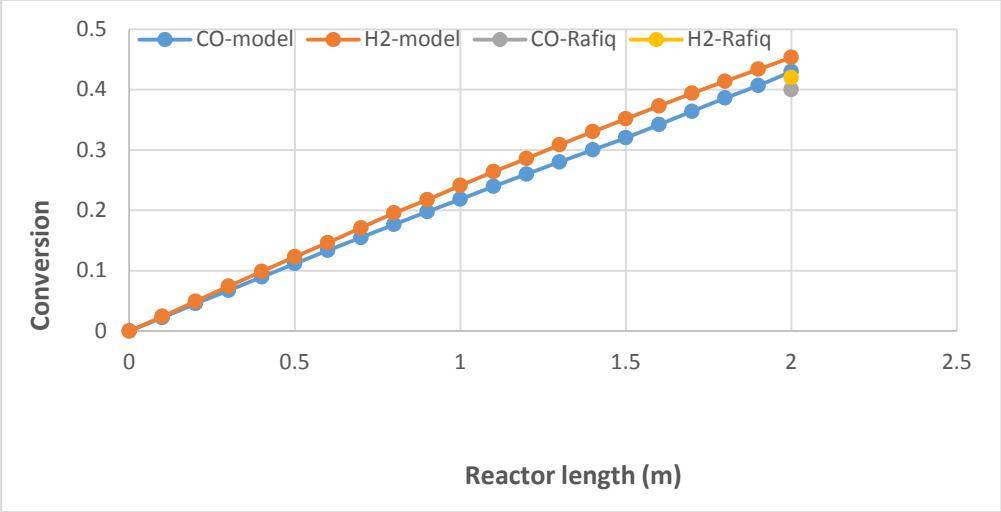

Figure 7. Syngas conversion along the reactor length.

5.2. Model validation

To evaluate the accuracy of the solution method, numerical simulation results were compared with theoretical and experimental results reported by Rafiq et al. [23] as given in Table 3.

Table 3
Comparison between the numerical results and the reported data by Rafiq [23].

Parameters	Pseudo-homogeneous model (Rafiq)	Experimental (Rafiq)	Heterogeneous model (This work)
X_{CO} (%)	50	40	43
X_{H_2} (%)	52	43	45.3
C_1 $(g.g_{cat}^{-1}.h^{-1})$	7.55×10^{-4}	5.71×10^{-4}	6.05×10^{-4}
C_2 $(g.g_{cat}^{-1}.h^{-1})$	1.47×10^{-4}	5.27×10^{-5}	5.54×10^{-5}
C_3 $(g.g_{cat}^{-1}.h^{-1})$	3.38×10^{-4}	1.54×10^{-4}	1.65×10^{-4}
C_4 $(g.g_{cat}^{-1}.h^{-1})$	3.64×10^{-4}	2.21×10^{-4}	2.21×10^{-4}
H_{2O} $(g.g_{cat}^{-1}.h^{-1})$	1.38×10^{-2}	1.10×10^{-2}	1.18×10^{-2}
C_{5+} $(g.g_{cat}^{-1}.h^{-1})$	9.59×10^{-3}	7.71×10^{-3}	8.33×10^{-3}

Table 3 shows that the predicted values of the conversion of carbon monoxide and hydrogen in this work are 43 and 45.3 percent, respectively, which are in good

agreement with the corresponding values of the experimental data. Furthermore, it shows that the deviations of predicted results of this work from the experimental data are 3 and 2.3 percent, respectively, compared to those of the pseudo-homogeneous (gas) model, which are 10 and 9 percent, respectively.

6. Conclusions

A comprehensive numerical study was conducted in order to investigate the effects of the liquid phase on the low-temperature FTS reactor. For this purpose, a 2D axisymetric heterogeneous (gas-liquid) model, rather than conventional pseudo-homogeneous models, was developed to simulate a fixed bed reactor in a trickle flow regime. To exert the influence of liquid film arround the catalyst pellets and its mass transfer restrictions, a mass transfer mechanism from gas to liquid phase was imposed. At the beginning of the process, there was no liquid in the reactor and the liquid phase was accumulated along the reactor axis during the time. Simultaneously, with the formation of the liquid phase, carbon monoxide and hydrogen dissolve in the liquid and will be out of reactions reach. As a result, the syngas concentration in gas phase will be reduced and leads to the less total conversion.

This reactor model was examined against the experimental and numerical pseudo-homogeneous model data. It was found that applying this model, instead of pseudo-homogeneous model, gives better results and decreases the errors of CO and H_2 conversion prediction from 25 % and 21 % to 7.5 % and 5 %, respectively.

According to what was mentioned above, pseudo-homogeneous model is not always an appropriate numerical model for applying in the LTFT synthesis.

Nomenclature

C_2	inertial resistance coefficient [m^{-1}].
d	diameter [m].
E	total energy [$kj.kg^{-1}$].
F	molar flow rate [$mol.s^{-1}$].
GHSV	gas hour space velocity [$Nml.g_{cat}^{-1}.h^{-1}$].
g	gravitational acceleration [$m.s^{-2}$].
h	enthalpy [$kj.kg^{-1}$].
j	mass flux [$kg.m^{-2}.s^{-1}$].
k	thermal conductivity [w.m-^{2}.k].
$\dot{m}$	mass transfer rate [$kg.m^{-3}.s^{-1}$].
Pr	productivity.
p	static pressure [pascal].
r	reaction rate [$mol.kg_{cat}^{-1}.s^{-1}$].
S	momentum sink term in momentum conservation equations [$kg.m^{-2}.s^{-2}$].
s	selectivity.
T	static temperature [k].
t	time [s].
$\vec{v}$	velocity vector [$m.s^{-1}$].
X	volume fraction.
Y	mass fraction.
x	conversion.
z	length direction [m].

Greek letters

α	permeability coefficient [m^2].
β	chains growth probability constant.
ε	bed prosity.
μ	viscosity [$kg.m^{-2}.s^{-1}$].
ρ	density [$kg.m^{-3}$].
$\bar{\bar{\tau}}$	shear stress tensor [$kg.m^{-2}.s^{-2}$].

Subscript and superscript

eff	effective
G	gas
i	ith specie
in	inlet
L	liquid
out	outlet
p	particle
s	solid
∞	free stream

References

[1] Hallac, B. B., K. K., Hedengren, J. D., Hecker, W. C. and Argyle, M. D., "An optimized simulation model for iron-based Fischer-Tropsch catalyst design: Transfer limitations as functions of operating and design conditions", *Chemical Engineering Journal*, **263**, 268 (2015).

[2] Pandey, S. K., CFD simulation of hydrodynamics of three phase fluidized bed in chemical engineering, National Institute of Technology, Rourkela, India, (2010).

[3] Guettel, T., R., "Comparison of different reactor types for low temperature Fischer-Tropsch synthesis: A simulation study", *Chemical Engineering Science*, **64**, 955 (2009).

[4] Magoo, A. K., Mittal, A. and Roy, S., "Modeling packed bed Fischer-Tropsch reactors with phase evolution", *Indian Chemical Engineer*, **55** (1), 29 (2013).

[5] Rahimpour, M. R., H. E., "Optimization of a novel combination of fixed and fluidized-bed hydrogen-permselective membrane reactors for Fischer-Tropsch synthesis in GTL technology", *Chemical Engineering Journal*, **152**, 543 (2009).

[6] Dai, X. P., et al., "Fischer-Tropsch synthesis in a bench-scale two-stage multitubular fixed-bed reactor: Simulation and enhancement in conversion and diesel selectivity", *Chemical Engineering Science*, **105** (0), 1 (2014).

[7] Atwood, H. E. and Bennett, C. O., "Kinetics of the Fischer-Tropsch reaction over iron", *Industrial & Engineering Chemistry Process Design and Development*, **18** (1), 163 (1979).

[8] Liu, Q. S., Z. X. Z., Zhou, J. L. and Zhang, B. J., "Heterogeneous modeling of fixed-bed Fischer-Tropsch synthesis: reactor model and It's applications", *Journal of Chemical Engineering Science*, **58**, 867 (2003).

[9] Wang, Y. -N., et al., "Heterogeneous modeling for fixed-bed Fischer-Tropsch synthesis: Reactor model and its applications", *Chemical Engineering Science*, **58** (3–6), 867 (2003).

[10] Jess, A., R. P. and Hedden, K., "Fischer-Tropsch synthesis with nitrogen-rich syngas: Fundamentals and reactor design aspects", *Applied Catalysis, A: General*, **186**, 321 (1999).

[11] Jess, A. and Kern, C., "Modeling of multi-tubular reactors for Fischer-Tropsch synthesis", *Chemical Engineering & Technology*, **32** (8), 1164 (2009).

[12] Lee, T. S., J. N. C., "Mathematical modeling and numerical simulation of a Fischer-Tropsch packed bed reactor and its thermal management for liquid hydrocarbon fuel production using biomass syngas", *Energy & Fuels*, **26**, 1363 (2012).

[13] Knochen, J., et al., "Fischer-Tropsch synthesis in milli-structured fixed-bed reactors: Experimental study and scale-up considerations", *Chemical Engineering and Processing: Process Intensification*, **49** (9), 958 (2010).

[14] Brunner, K. M., H. D. P., Peguin, R. P. S., Duncan, J. C., Harrison, L. D., Bartholomew, C. H. and Hecker, W. C., "Effects of particle size and shape on the performance of a trickle fixed-bed recycle reactor for Fischer-Tropsch synthesis", *Industrial & Engineering Chemistry Research*, **54**, 2902 (2015).

[15] Lee, T. -S., Numerical modeling and

simulation of Fischer-Tropsch packed bed reactor and its thermal managment, in Chemical Engineering, University of Florida, (2011).

[16] Rytter, E., N. E. T. and Holmen, A., "On the selectivity to higher hydrocarbons in co-based Fischer-Tropsch synthesis", *Catalysis Today*, **261**, 3 (2015).

[17] Vervloet, D., F. K., Nijenhuis, J. and van Ommen, J. R., "Fischer-Tropsch reaction-diffusion in a cobalt catalyst particle: aspects of activity and selectivity for a variable chain growth probability", *Catalysis Science and Technology*, **2**, 1221 (2012).

[18] Benyahia, F., K. E. O. N., "Enhanced voidage correlations for packed beds of various particle shapes and sizes", *Particulate Science and Technology*, **23**, 169 (2005).

[19] Fratalocchi, L., C. G. V., Lietti, L., Tronconi, E. and Rossini, S., "Exploiting the effects of mass transfer to boost the performances of Co/-Al_2O_3 eggshell catalysts for the Fischer-Tropsch synthesis", *Applied Catalysis, A: General*, **512**, 36 (2016).

[20] Wang, Y. -N., et al., "Modeling of catalyst pellets for Fischer-Tropsch synthesis", *Industrial & Engineering Chemistry Research*, **40** (20), 4324 (2001).

[21] Visconti, C. G., E. T., Groppi, G., Lietti, L., Iovane, M., Rossini, S. and Zennaro, R., "Monolithic catalysts with high thermal conductivity for the Fischer-Tropsch synthesis in tubular reactors", *Chemical Engineering Journal*, **171**, 1294 (2011).

[22] Brunner, K. M., J. C. D., Harrison, L. D., Pratt, K. E., Peguin, R. P. S., Bartholomew, C. H. and Hecker, W. C., "A trickle fixed-bed recycle reactor model for the Fischer-Tropsch synthesis", *International Journal of Chemical Reactor Engineering*, **10**, (2012).

[23] Rafiq, M. H., H. A. J., Schmid, R. and Hustad, J. E., "Experimental studies and modeling of a fixed bed reactor for Fischer-Tropsch synthesis using biosyngas", *Fuel Processing Technology*, **92**, 893 (2011).

[24] Ermolaev, V. S., K. O. G., Mitberg, E. B., Mordkovich, V. Z. and Tretyakov, V. F., "Laboratory and pilot plant fixed-bed reactors for Fischer-Tropsch synthesis: Mathematical modeling and experimental investigation", *Chemical Engineering Science*, **138**, 1 (2015).

[25] Steynberg, A. P. D., M. E., Davis, B. H. and Breman, B. B., "Fischer-Tropsch reactors", *Studies in Surface and Catalysis*, **152**, (2004).

[26] Kamali, M. R., A lattice Boltzmann approach to multi-phase surface reactions with heat effects, Technische Universiteit Delft, (2013).

[27] Ahmadi Marvast, M., M. S., Zarrinpashneh, S. and Baghmisheh, G. R.,"Fischer-Tropsch synthesis: Modeling and performance study for Fe-HZSM5 bifunctional catalyst", *Chemical Engineering Technology*, **28** (1), (2005).

[28] Philippe, R. M. L., Dreibine, L., Huu, C. P., Edouard, D., Savin, S. and Luck, F., "Effect of structure and thermal properties of a Fischer-Tropsch catalyst in a fixed bed", *Catal. Today*, **147**, 305 (2009).